

Bifunctional Ruthenium Catalysts for *endo*-Selective Cycloisomerization of Nucleophile-Functionalized Terminal Alkynes

Garcia Mayerstein, H. A.; Song, D.

Version Post-print/Accepted Manuscript

Citation (Published Version) Garcia Mayerstein, H. A.; Song, D. Bifunctional Ruthenium Catalysts for *endo*-Selective Cycloisomerization of Nucleophile-Functionalized Terminal Alkynes. *ACS Catalysis* **2024**, *14* (23), 17489–17502.

DOI <https://doi.org/10.1021/acscatal.4c05245>

Publisher's Statement This document is the Accepted Manuscript version of a Published Work that appeared in final form in ACS Catalysis, copyright © 2024 American Chemical Society after peer review and technical editing by the publisher. To access the final edited and published work see <https://doi.org/10.1021/acscatal.4c05245>.

How to cite TSpace items

Always cite the published version, so the author(s) will receive recognition through services that track citation counts, e.g. Scopus. If you need to cite the page number of the **author manuscript from TSpace** because you cannot access the published version, then cite the TSpace version **in addition** to the published version using the permanent URI (handle) found on the record page.

**This article was made openly accessible by U of T Faculty.
Please tell us how this access benefits you. Your story matters.**

Bifunctional ruthenium catalysts for *endo*-selective cycloisomerization of nucleophile-functionalized terminal alkynes

Hector A. Garcia Mayerstein and Datong Song*

Davenport Chemical Research Laboratories, Department of Chemistry, University of Toronto, 80 St. George Street, Toronto, Ontario, Canada M5S 3H6

ABSTRACT: The catalytic cycloisomerization of nucleophile-functionalized alkynes is a useful method for the synthesis of heterocyclic compounds with 100% atom economy. Group 8 catalysts give high *endo*-selectivity in these transformations due to their ability to invoke metal-vinylidene intermediates. However, all known group 8 catalysts have relatively low activities and require high temperatures. Here we report bifunctional ruthenium catalysts that enable the cycloisomerization of a large variety of substrates at low catalyst loadings and ambient temperature with turnover frequencies as high as 200 s⁻¹.

KEYWORDS: Ruthenium, alkyne, *endo*-selective, cycloisomerization, metal-ligand cooperation, catalysis, vinylidene, heterocycle synthesis

INTRODUCTION

Heterocycles are prevalent structural motifs in natural products, pharmaceuticals, agrochemicals, colorants, and luminescent materials.¹⁻⁴ Much research effort has been expended in search of a versatile method that enables the synthesis of a large variety of heterocyclic compounds under mild conditions with high selectivity and atom economy. The catalytic cycloisomerization of nucleophile-functionalized alkynes is a powerful method for the construction of heterocyclic compounds with 100% atom economy.^{5,6} When metal-vinylidene intermediates are involved, these reactions give extremely high *endo*-selectivity owing to the electrophilicity of the α -carbon of the vinylidene ligand.⁶⁻⁸ Utilizing this mechanistic pathway, the McDonald group pioneered the *endo*-selective reactions using photochemically generated organic amine adducts of group 6 metal carbonyl complexes as the catalysts.^{9,10} In contrast, coinage metal catalysis generally operates via nucleophilic attack of π -bound alkynes,^{11,12} where *endo*-selectivity is challenging to achieve and often limited to the formation of five-membered rings.

Although McDonald's method has been successfully applied to multistep syntheses,¹³⁻¹⁸ the needs for extremely high catalyst loadings, added base, and various conditions for catalyst activation call further catalyst development. Trost reported a Rh-catalyzed cycloisomerization of alkynols^{19,20} and alkynamines²¹ to afford five- and six-membered rings at 85 °C. Lee extended the Rh-catalyzed reactions to alkynes with pendent enamine nucleophiles.²² Catalysts based on group 8 metals have outnumbered other catalysts for such transformations,^{23,24} since the early reports by Trost²⁵ and Saá²⁶⁻²⁸ on half-sandwich Ru catalysts. The related cationic half-sandwich Os catalysts by Esteruelas and Saá can cycloisomerize phenylacetylenes with pendent alcohol²⁹ or amine³⁰ functional groups at the *ortho* position into 6,7-fused ring systems at a 10 mol% catalyst loading using pyridine as the base and solvent at 90 °C. In contrast, a related piano-stool bimetallic Ru/Au catalyst dimerizes 2-ethynylaniline to a qui-

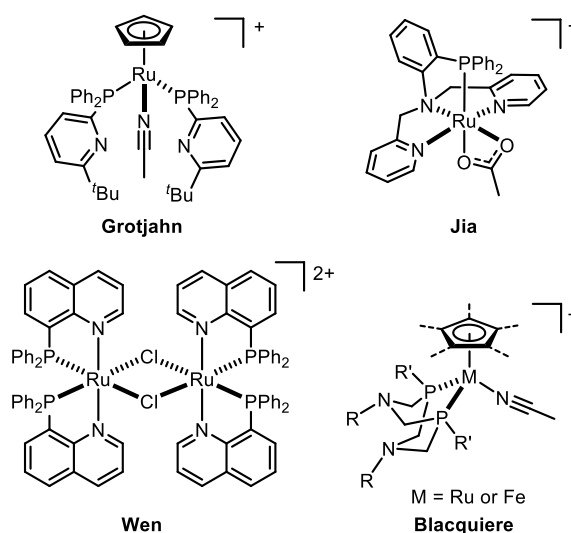


Chart 1. Bifunctional group 8 catalysts for *endo*-selective cycloisomerization of nucleophile-tethered terminal alkynes.

noline derivative instead.³¹

The introduction of a built-in base into catalyst design eliminates the need for stoichiometric base (Chart 1). For example, Grotjahn's cationic bifunctional [CpRuL₂(CH₃CN)]⁺ catalyst (where L = 2-(*tert*-butyl)-6-(diphenylphosphanyl)pyridine), originally used for the *anti*-Markovnikov hydration of alkynes,³² can effect the formation of indoles and benzofurans, from *o*-amino and hydroxyphenylacetylenes, respectively, at 70 °C at 2–5 mol% catalyst loading.^{33,34} Jia reported a cationic [Ru(N₃P)(OAc)]⁺ catalyst (where N₃P = 2-(diphenylamino)methyl-1-diphenylphosphino-1H-benzene), which can cycloisomerize a wide range of alkynols into the corresponding 5-, 6-, and 7-membered rings in excellent yields using 1–5 mol% catalyst loadings at 80 °C.³⁵ Wen and coworkers reported a dicationic dinuclear Ru pre-catalyst featuring bidentate P,N-donor ligands, which is believed to disso-

ciate into monomers to effect catalysis at a 1 mol% catalyst loading (i.e., equivalent to a 2 mol% loading of Ru) at 90 or 100 °C.³⁶ The Blacquiere group employed macrocyclic P_2N_2 -ligands to construct a series of cationic half-sandwich Ru precatalysts toward the cycloisomerization reaction; with the dangling amine of the P_2N_2 -ligand shuttling protons in catalysis, the catalytic reaction can proceed at 70 °C at 0.5–5 mol% catalyst loadings for closing 5- and 6-membered rings.^{37–39} The same group also reported analogous half-sandwich Fe precatalysts, which can cycloisomerize 2-ethynylbenzyl alcohol into isochromene at 110 °C.⁴⁰

Although no stoichiometric base is needed, the above catalysts show low activities and thus require elevated temperatures. Two common features shared by all these (pre)catalysts above may be responsible for the low catalytic activities: (1) cationic, i.e., the counteranion may interfere with substrate binding; (2) coordinatively saturated, i.e., ligand dissociation is needed prior to catalysis. In search of highly active catalysts that can operate under mild conditions, we set to develop charge-neutral and coordinatively unsaturated catalysts with suitable built-in base. Our group has developed MCycNHC catalysts (where M = Fe or Ru) (Chart 2) for the dimerization of terminal alkynes, where the strong inner-sphere built-in base (i.e., cyclometallated mesityl) can deprotonate the alkyne σ -complexes to form metal-alkynyl intermediates and free up its original coordination site for further alkyne coordination.^{41–44} It is conceivable that a weaker built-in base should be able to deliver the proton back to the β -carbon of the resulting alkynyl ligand to facilitate the formation of vinylidene, which typically is an energetically demanding step.^{45,46} The weaker built-in base would also help shuttle protons in the subsequent ring closure and product releasing steps. We envision that the 2-pyridone motif would have the suitable basicity and geometry^{47,48} for this task as its ability to act as a ligand-based proton shuttle has been reported in transition metal and main group catalysts.^{49–57} Particularly, the 2-pyridone motif have been used to activate the C–H bond of terminal alkynes (Chart 2). For instance, Wang and coworkers reported a monomeric Co(II) piano-stool phosphinepyridonato catalyst capable of the sequential *E*-selective dimerization of terminal aryl alkynes and partial reduction of the resulting 1,3-enynes into (*E,Z*)-1,3-dienes with excellent stereoselectivity.⁵⁵ Gellrich's boroxypyridine catalyst displays moderate activity toward *gem*-selective alkyne dimerization.⁵⁶ Castarlenas reported *gem*-selective alkyne dimerization catalyzed by Rh(2-pyridonato)NHC with extremely high activity and selectivity.⁵⁷ The ability of the 2-pyridonato ligand to engage in metal–ligand cooperative proton transfer is suggested to be responsible for the catalytic activity. Herein we report two new charge-neutral Ru complexes of monoanionic *N,C*-chelate ligands, featuring the 2-pyridone motif. These well-defined complexes can effect the *endo*-selective cycloisomerization of a wide range of nucleophile-functionalized terminal alkynes at ambient temperatures.

RESULTS AND DISCUSSION

Complexes **Ru1** and **Ru2** were synthesized as purple solids in high yields by reacting $[\text{Cp}^*\text{RuCl}]_4$ with the *in situ* generated **L1** and **L2**, respectively (Scheme 1). The molecular structures of **Ru1** and **Ru2** were revealed by X-ray crystallography. As shown in Figure 1, **Ru1** and **Ru2** feature the half-sandwich geometry, where each Ru center is ligated by an η^5 -Cp* ligand

and an *N,C*-chelate ligand, displaying typical metric parameters.⁵⁸ Each metal center has a vacant coordination site, where agostic interactions were found with the methyl C–H of the wingtip aryl group (C–Ru distance: ~ 3.5 Å in **Ru1** and ~ 3.2 Å in **Ru2**). The oxygen atom of the bidentate ligand is dangling

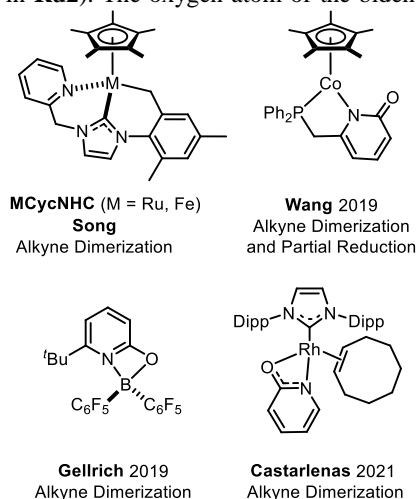
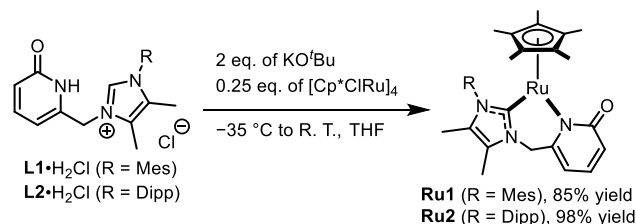


Chart 2. Our alkyne dimerization catalysts (top left) and literature catalysts containing pyridone moieties (rest).



Scheme 1. Syntheses of **Ru1** and **Ru2**.

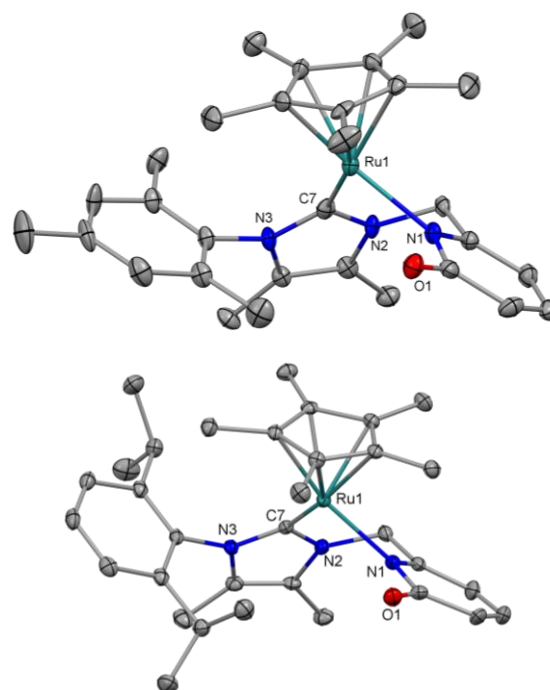
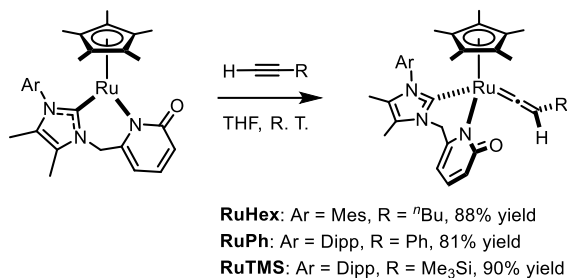


Figure 1. X-ray structures of **Ru1** (top) and **Ru2** (bottom) with thermal ellipsoids shown at 30% probability level. Hydrogen atoms are omitted for clarity.

adjacent to the vacant site of the Ru center. The ^1H NMR spectra of **Ru1** and **Ru2** in C_6D_6 have the characteristic AB pattern signals from the bridging CH_2 group of the chelate ligand, (**Ru1**: 4.27 and 4.23 ppm ($^2J_{\text{H-H}} = 13.5$ Hz); **Ru2**: 4.40 and 4.24 ppm ($^2J_{\text{H-H}} = 13.6$ Hz)). In the ^{13}C NMR spectra, the carbene carbon resonances appear at 199.9 and 200.4 ppm for **Ru1** and **Ru2**, respectively.



Scheme 2. Reactivity of Ru1 and Ru2 toward terminal alkynes.

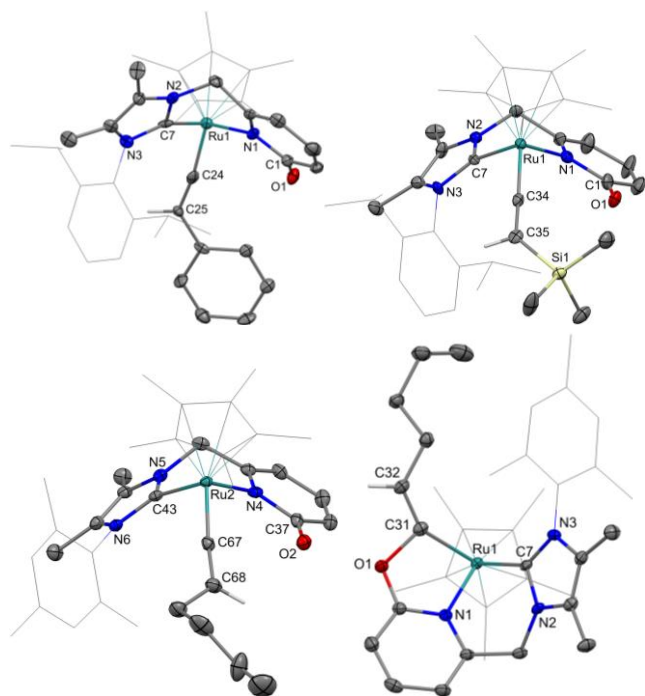


Figure 2. X-ray structures of vinylidene complexes with thermal ellipsoids shown at 30% probability level. Hydrogen atoms except for those on the C_β of vinylidenes are omitted and Cp^* and the wingtip aryl groups are shown as wireframe for clarity. **RuPh** (top left), **RuTMS** (top right), **RuHex** (bottom left) and **RuHex'** (bottom right).

As shown in Scheme 2, **Ru1** and **Ru2** react instantaneously with terminal alkynes to form the corresponding vinylidene complexes. The new vinylidene complexes **RuPh**, **RuTMS**, and **RuHex** can be isolated in high yields. **RuPh** and **RuHex** are fluxional in C_6D_6 solution at 25 $^\circ\text{C}$ showing broad ^1H resonances for the proton on the C_β of the vinylidene ligands at 3.37 and 3.57 ppm, respectively. Additionally, broad signals were observed for the ring protons of the phenylvinylidene ligand and protons of the Dipp group in **RuPh** as well as the protons on the C_7 of the vinylidene ligand in **RuHex**. All signals of **RuPh** and **RuHex** sharpen upon cooling to -80 $^\circ\text{C}$ in $\text{THF-}d_8$ solution. The ^1H NMR spectrum of **RuTMS** shows sharp signals indicating a rigid environment around the

molecule. The line-shape analyses^{59,60} of the ^1H NMR signals of **RuPh** and **RuHex** reveal that the free energy barriers of the processes causing the broadening are 14.8 ± 1.3 and 13.5 ± 0.7 kcal mol^{-1} , respectively. This broadening is tentatively attributed to the rotation of the vinylidene moiety around the C-C-Ru axis, based on the computed free energy barriers of 14.4 and 11.2 kcal mol^{-1} for **RuPh** and **RuHex**, respectively (see the Supporting Information). The tautomerization between the alkynyl and vinylidene complexes also has similar computed barrier; the dynamic solution behavior of **RuPh** and **RuHex** caused by such a process cannot be ruled out. In the ^{13}C NMR spectra, the vinylidene C_α resonances (343.7, 332.6, and 332.8 ppm for **RuHex**, **RuPh**, and **RuTMS**, respectively) are similar to those of reported charge neutral Ru vinylidene complexes.^{60–63} The carbene carbons of the NHC ligands of **RuPh**, **RuHex**, and **RuTMS** resonate at 187.9, 189.7, and 193.8 ppm, respectively, consistent with the trend in the electron-donating ability of the three vinylidene ligands.

X-ray crystallography confirms the three-legged piano stool structures of all three vinylidene complexes in the solid state (Figure 2). For the Ru-vinylidene fragments of all three complexes, the Ru-C_α and $\text{C}_\alpha\text{-C}_\beta$ bond lengths and $\text{Ru-C}_\alpha\text{-C}_\beta$ angles are similar to those found in known Ru-vinylidene compounds.^{61,62} In **RuPh** and **RuTMS**, the substituent on the vinylidene moiety points away from the Dipp wingtip group. In **RuHex** the substituent on the vinylidene moiety is on the Mes wingtip group side, which could be attributed to crystal packing effects, because computed the free energy difference of the two conformers is only 0.2 kcal mol^{-1} and the one with alkyl substituent away from the Mes group is slightly more stable (see the Supporting Information). The pyridone C–O bond lengths in **RuPh**, **RuTMS**, and **RuHex** are 1.243(9), 1.25(1), and 1.237(6) Å, respectively, typical for C–O double bonds. Interestingly, **RuHex** cocrystallized with its isomer **RuHex'** in a 1:1 molar ratio. Compared to **RuHex**, **RuHex'** features an O–C bond between the pyridone oxygen and the C_β of the vinylidene ligand, with a bond length of 1.548(6) Å significantly longer than a typical C–O single bond and close to those found in oxonium salts.⁶⁴ Compared to the metric parameters for **RuHex**, the pyridone C–O and Ru-C_α bonds are significantly elongated to 1.316(6) and 2.051(6) Å from 1.237(6) and 1.813(5) Å, respectively. **RuHex'** was not observed in the solution NMR spectrum of **RuHex**. DFT calculations show that **RuHex'** is less stable than **RuHex** by 0.6 kcal mol^{-1} in terms of free energy and the free energy barrier from **RuHex** to **RuHex'** is 6.8 kcal mol^{-1} (see the Supporting Information), much lower than the vinylidene rotation barrier (*vide supra*), i.e., this fast process might not be the main contributor to the line broadening of the ^1H NMR spectrum of **RuHex**.

Bullock reported the isomerization of $[\text{CpRu}(\text{PMe}_3)_2(\eta^2\text{-propyne})]^+$ into the corresponding vinylidene complex, which has an experimentally-measured Gibbs free energy barrier of ~ 22 kcal mol^{-1} at 298 K.⁶⁵ The mechanism of this reaction has been computed by Wakatsuki, showing that the intramolecular 1,2-proton shift pathway is likely responsible for this transformation.⁶⁶ We computed the energetics of the intramolecular 1,2-proton shift pathway for the reaction of **Ru1** and 1-hexyne, which has a free energy barrier of 24.5 kcal mol^{-1} (see Figure S164) similar to Wakatsuki's computational result and Bullock's experimental result. However, a free energy barrier of 24.5 kcal mol^{-1} is too high

for an instantaneous reaction at room temperature. Interestingly, we found another reaction pathway with a free energy barrier of only 14.8 kcal mol⁻¹, which involves the intramolecular deprotonation of the alkyne σ -complex by the pyridone oxygen of the chelate ligand and the subsequent delivery of the proton to the C β of the resulting alkynyl ligand (see the Supporting Information). In fact, the rate-limiting transition state along this pathway is the formation of the σ -complex from the η^2 -alkyne complex. Clearly, the participation of the actor ligand can lower the free energy barrier by nearly 10 kcal mol⁻¹. The related outer-sphere N-donor-assisted formation of Ru-vinylidene was reported for the catalytic hydration of alkynes,^{32,67,68} where the pendent pyridine or imidazole N-donors are believed to facilitate intramolecular proton transfer. In addition, the more basic imidazole N-donor also attacks the C α of vinylidene, leading to the formation of the cyclized product in solution.

The facile formation of vinylidene complexes from terminal alkynes has prompted us to examine the catalytic activity of **Ru1** toward the cycloisomerization of nucleophile-functionalized alkynes. **Ru1** shows excellent catalytic activity for a variety of aromatic and aliphatic substrates (Table 1). With a 1 mol% catalyst loading, *o*-hydroxyphenylacetylene can be cleanly converted to benzofuran (**C1**) within a few seconds at ambient temperature, even in the presence of a sensitive aldehyde functional group (**C2**). For the homologous benzyl alcohol substrate, the catalytic formation of isochromene (**C3**) is equally facile. Bulking up the benzyl alcohol does not retard the catalysis as evidenced by the instantaneous formation of substituted isochromenes **C4–C6**. The acidic 2-ethynylbenzoic acid is also compatible with the catalyst, resulting in a quantitative formation of isocoumarin (**C7**) within a minute. Tricyclic compound **C8** can also be efficiently and instantaneously obtained under the same catalytic conditions (i.e., equivalent to 0.05 mol% per cyclizable moiety), the rate of dissolution of the starting material being slower than the catalysis itself. Benzooxaborininol **C9** can be obtained from the cyclization of 2-ethynylboronic acid in quantitative yield in the presence of a small amount of water, which can convert the cyclic trimer of the boronic acid into cyclizable monomer. If the reaction is conducted with mostly the cyclic trimer of 2-ethynylboronic acid under anhydrous conditions, the yield is considerably lowered (see the Supporting Information). This type of reactivity is rare for boronic acids; to the best of our knowledge, there is only one report of a similar palladium-catalyzed cyclization in the literature.⁶⁹ Compared to the phenylacetylene derivatives, the aliphatic alkynols are significantly less reactive. Under the standard conditions, 4-pentyn-1-ol can be quantitatively converted to **C10** in 1.5 h, much slower than the formation of all the aromatic analogues **C3–C6**. The Ru-catalyzed cyclization of 3-butyne-1-ol into dihydrofuran has been reported as a challenging reaction, which requires higher catalyst loadings, longer reaction time, and gives lower yields compared to the related formation of benzofuran.^{35,36} The formation of dihydrofurans **C11** and **C12** reaches completion with quantitative yields in 10 h at 80 °C with a 1 mol% catalyst loading of **Ru1**. The closure of seven-membered rings to form benzooxepins (**C13** and **C14**) reaches completion with quantitative yields in 1.5 h at ambient temperature with a 1 mol% catalyst loading. Using a carboxylic acid nucleophile in lieu of the alcohol slows down the reaction significantly, i.e., the quantitative formation of

C15 takes 24 hours under the same conditions. Remarkably, the quantitative formation of aliphatic 7-membered ring, oxepin **C16**, can be achieved under the same conditions in 30 h. Closing 8-membered rings is even more challenging than the formation of dihydrofurans due to entropic effects. The formation of dibenzooxocin **C17** gives nearly quantitative yield in 24 h at 80 °C and 3 mol% loading. In contrast, the aliphatic 8-membered ring, oxocin **C18**, can only be produced in low yields under the same conditions; significant decomposition of the starting material is evident by NMR spectroscopy. The cyclization of propargyl salicylate was also tested, however, no oxocin product formation was detected even after 48 h at 80 °C with a 3 mol% loading of **Ru1** (see the Supporting Information). In all cases above, there is a marked difference in reactivity between arylacetylenes and their aliphatic counterparts, whereas alkyl groups adjacent to the nucleophile make no difference.

To illustrate the importance of the pyridone moiety, other charge-neutral RuCp*NHC complexes (Figures S73–S76) were tested for the conversion of 2-ethynylbenzyl alcohol to **C3**. For example, the reaction catalyzed by 3 mol% of **RuCp*Cl(IMes)**⁷⁰ only gives a trace of **C3** in 1 h at room temperature, along with unreacted substrate; when 3 mol% of **RuCp*Cl(IMes)** was used in combination with 3 mol% of LiHMDS, **C3** was produced in ~9% yield in 1 h, along with 1,3-enynes as the major products.⁴¹ The reaction catalyzed by 3 mol% of **RuCycNHC**⁵⁸ (Chart 2) gives **C3** in ~10% yield 1 h at room temperature, along with traces of 1,3-enynes. Clearly, none of these complexes without the pyridone motif is as active or selective as **Ru1**.

The catalytic system shows excellent functional group tolerance, evidenced by the fast and clean formation of a variety of indoles **C19–C26** at a 1 mol% loading of **Ru1** and ambient temperature. With the same catalyst loading, the cyclization of the aliphatic substrate 1-amino-3-butyne on the other hand takes 4 days to reach completion at 80 °C, affording the cyclic imine **C27** in quantitative yield; no enamine product was detected in the reaction mixture presumably due to thermal isomerization to the corresponding cyclic imine. Primary and secondary amides can be efficiently cyclized (**C28** and **C29**) despite their low nucleophilicity. The formations of an unprotected 7-membered cyclic enamine **C30** and the fused ring system in **C31** further demonstrate the utility of our catalytic method. The cyclization of an oxime derivative results in the formation of the corresponding isoquinoline *N*-oxide **C32**, likely due to the preferential nucleophilic attack of the nitrogen atom on the vinylidene intermediate; in this case, the acidic proton is not directly bonded to the N atom but the adjacent O atom. If an imine *N*-oxide analogue of the oxime is subjected to the catalytic conditions, no product formation is observed presumably due to the lack of acidic proton near the nucleophilic oxygen (see the Supporting Information). A thiol nucleophile is also compatible with our catalyst, evidenced by the instantaneous quantitative formation of 1H-isothiochromene **C33** from (2-ethynylphenyl)methanethiol at ambient temperature with a 1 mol% loading of **Ru1**. To the best of our knowledge, the only other example of cycloisomerization involving thiol nucleophile is the related dihydrothiophene formation, which requires stoichiometric amounts of group 6 carbonyl complexes and base under photolysis conditions, this presents the first example of an intramolecular alkyne hydrothiolation under mild conditions.⁷¹

Table 1. Ru1-catalyzed cycloisomerization of nucleophile-functionalized alkynes.

Standard Conditions ^a					
O-Nucleophiles					
C1 ≥ 99%, < 1 min	C2 ≥ 99%, ^b < 1 min	C3 ≥ 99%, < 1 min	C4 ≥ 99%, < 1 min	C5 ≥ 99%, ^b < 1 min	C6 ≥ 99%, ^b < 1 min
C7 ≥ 99%, < 1 min	C8 99%, ^{b,c} < 1 min	C9 ≥ 99%, ^d 10 min	C10 ≥ 99%, 1.5 h	C11 ≥ 99%, ^e 10 h	C12 ≥ 99%, ^e 10 h
C13 ≥ 99%, ^b 1.5 h	C14 ≥ 99%, ^b 1.5 h	C15 ≥ 99%, ^b 24 h	C16 ≥ 99%, 30 h	C17 98%, ^{b,c,e,f} 24 h	C18 20%, ^{e,f} 24 h
N/S-Nucleophiles					
C19 ≥ 99%, < 1 min	C20 ≥ 99%, ^b < 1 min	C21 ≥ 99%, ^b < 1 min	C22 ≥ 99%, ^b < 1 min	C23 ≥ 99%, ^b < 1 min	
C24 99%, ^{b,g} < 1 min	C25 ≥ 99%, ^b 2 min	C26 ≥ 99%, ^b < 1 min	C27 ≥ 99%, ^e 4 d	C28 ≥ 99%, 2 min	
C29 ≥ 99%, ^{b,e} 45 min	C30 ≥ 99%, ^b 8 h	C31 ≥ 99%, ^b 8 h	C32 ≥ 99%, ^b 6 h	C33 ≥ 99%, ^b < 1 min	

^a Substrate (0.20 mmol), Ru1 stock solution (0.5 mL, 4.0 mmol L⁻¹ in THF) and mesitylene (0.20 mmol) as the internal standard at room temperature; yields determined by the integration of ¹H NMR signals relative to the internal standard.

^b Isolated yield; no internal standard was added.

^c Preparative scale reaction also conducted (0.5 to 1.0 mmol scale).

^d A drop of degassed water was added.

^e At 80 °C.

^f 3 mol% catalyst loading achieved using a Ru1 stock solution (0.5 mL, 12.0 mmol L⁻¹ in THF).

^g Isolated yield at 50.0 mmol scale, 0.1 mol% catalyst loading.

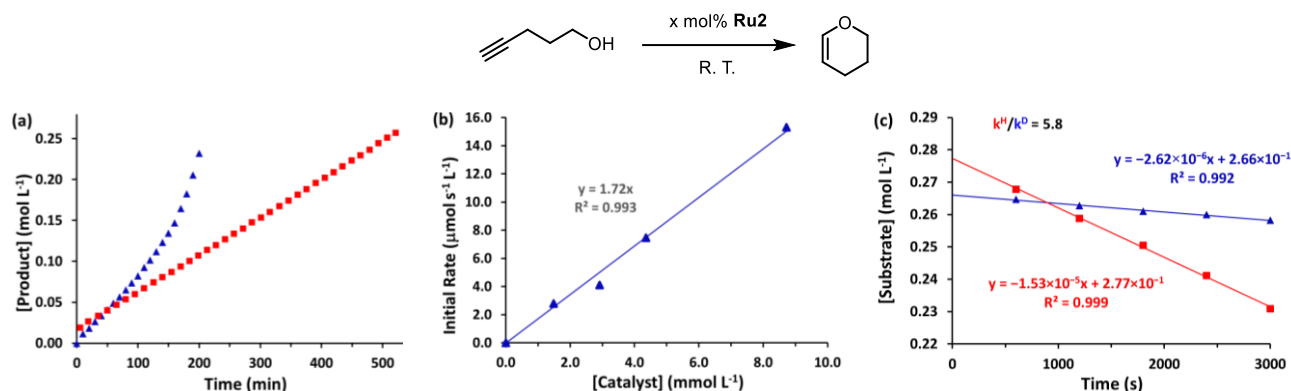


Figure 3. Kinetic data. (a) Reaction profile of cycloisomerization of 4-pentyn-1-ol catalyzed by 3 mol% of **Ru2** in C₆D₆ at 298 K with (■) and without (▲) additional 1-hexanol (5 equiv. wrt 4-pentyn-1-ol); (b) initial rate vs catalyst concentration plot; (c) initial reaction profile for the cycloisomerization of 4-pentyn-1-ol (■) and 4-pentyn-5-*d*-1-ol-*d* (▲).

To probe the reaction mechanism with ¹H NMR spectroscopy, we chose the cycloisomerization of 4-pentyn-1-ol catalyzed by **Ru2** as the model because its relatively slow rate (i.e., at 1 mol% catalyst loading, the reaction takes ~20 h to reach completion; Table S1) at 298 K makes monitoring the reaction progress by NMR spectroscopy convenient. The reaction rate stays constant (i.e., zeroth order in substrate concentration) up to ~40% conversion and then keeps increasing till the completion of the reaction (Figure 3a, blue trace). The zeroth order in substrate concentration could be attributed to the facile saturation of the catalyst's active site, given that the catalyst is able to convert terminal alkynes into vinylidene complexes instantaneously. Regarding the rate increase after 40% conversion, it is conceivable that the alcohol functional group of the substrate could hydrogen bond with the pyridone oxygen (at both protonation states) reversibly, retarding the pyridone-assisted proton shuttling processes; as the concentration of the free substrate decreases below a certain threshold, the reaction rate increases. Indeed, in the presence of excess 1-hexanol, a model retardant, the catalytic reaction rate is significantly slower and stays constant throughout the entire course of the reaction (Figure 3a, red trace). The reaction rate shows first-order dependence on the catalyst concentration within the range of 0–8.72 mmol L⁻¹ (Figure 3b). When 4-pentyn-5-*d*-1-ol-*d* is used as the substrate, the reaction gives 3,4-dihydro-2*H*-pyran-5,6-*d*₂ (**C10-d**₂) selectively (see the Supporting Information) at a significantly slower rate, displaying a normal primary KIE of 5.8 (Figure 3c). Interestingly, when using 4-pentyn-5-*d*-1-ol as the substrate, isotopic scrambling is seen with 50% D incorporation at both olefinic positions of the product (see the Supporting Information). We tentatively propose that such H-D exchange takes place prior to vinylidene formation, given that vinylidene complex **RuHex** shows no noticeable H-D exchange with excess CD₃OD in THF-*d*₈ solution within 24 h at room temperature (Figures S158, S159).

The reaction mechanism was also explored using DFT calculations (Figure 4). The coordination of the alkyne moiety of the substrate gives intermediate **A** (7.0 kcal mol⁻¹), which undergoes slippage to give the σ-complex intermediate **B** (7.1 kcal mol⁻¹) via transition state **TS_{AB}** (10.7 kcal mol⁻¹). The pyridone oxygen deprotonates intermediate **B** to afford an alkynyl complex **C** (4.8 kcal mol⁻¹) via transition state **TS_{BC}** (7.2 kcal mol⁻¹). Subsequently, the pyridone delivers the proton to the C_β of the alkynyl ligand to give vinylidene

complex **D** (−5.7 kcal mol⁻¹) via transition state **TS_{CD}** (9.5 kcal mol⁻¹). The rotation of the initially formed vinylidene goes through **TS_{DE}** (4.4 kcal mol⁻¹) giving intermediate **E** (−10.8 kcal mol⁻¹), where the dangling alcohol functional group of the vinylidene ligand can hydrogen bond to the pyridone oxygen. Intermediate **E** can then undergo concerted deprotonation and C–O bond formation to close the six-membered ring and give intermediate **F** (−7.0 kcal mol⁻¹) via transition state **TS_{EF}** (5.9 kcal mol⁻¹). The pyridone oxygen can deliver the proton back to the C_α of the vinyl ligand to release the product from the metal center and regenerate **Ru2** via transition state **TS_{Fru2}** (5.8 kcal mol⁻¹). Up to this point, the energetic span of the catalytic cycle seems to be 16.7 kcal mol⁻¹ (i.e., between **E** and **TS_{EF}**), which means the reaction should reach completion in minutes at 298 K rather than 20 h experimentally (Table S1). However, **F** could undergo another low-barrier process that is competing with product release: the proton delivery from the pyridone oxygen to C_β via **TS_{FG}** (3.2 kcal mol⁻¹), yielding an off-cycle alkoxycarbene complex **G** (−15.7 kcal mol⁻¹) which is more stable than **F**. Therefore, the energetic span of the catalytic reaction is 21.5 kcal mol⁻¹ (i.e., between **G** and **TS_{Fru2}**). When 4-pentyn-5-*d*-1-ol-*d* is the substrate, the energetic span becomes 22.5 kcal mol⁻¹ (**TS_{Fru2-d2}**: 6.8 kcal mol⁻¹ and **G-d2**: −15.7 kcal mol⁻¹), which translates to a normal primary KIE of 5.4, consistent with the experimental data. The computed ΔG^o of the overall reaction is −27.3 kcal mol⁻¹, which gives enough driving force for the off-cycle species **G** to isomerize back to **F** and release the product, regenerating **Ru2**. Based on these results, **Ru2** can be quickly converted to **G** under catalytic conditions, consistent with the saturation kinetics observed experimentally. It is conceivable that the coordinated substrate in intermediate **A** might undergo cyclization and transfer the alcohol proton to the pyridone ligand to produce **A'**, which could then release the product and regenerate **Ru2**. However, the free energy of **A'** is 20.0 kcal mol⁻¹, which is higher than the highest transition state **TS_{AB}** in the route above. Therefore, this alternative route is considered uncompetitive and not examined further.

In contrast to the relatively slow catalytic formation of **C10**, the formation of **C3** catalyzed by **Ru2** reaches completion within a minute (Table S1), consistent with the general trend observed for **Ru1**. To understand the origin of such a difference between aryl and aliphatic acetylenes, we computed the free energy profile of the catalytic formation of **C3** (Figure S166). The first major difference along the computed pathway

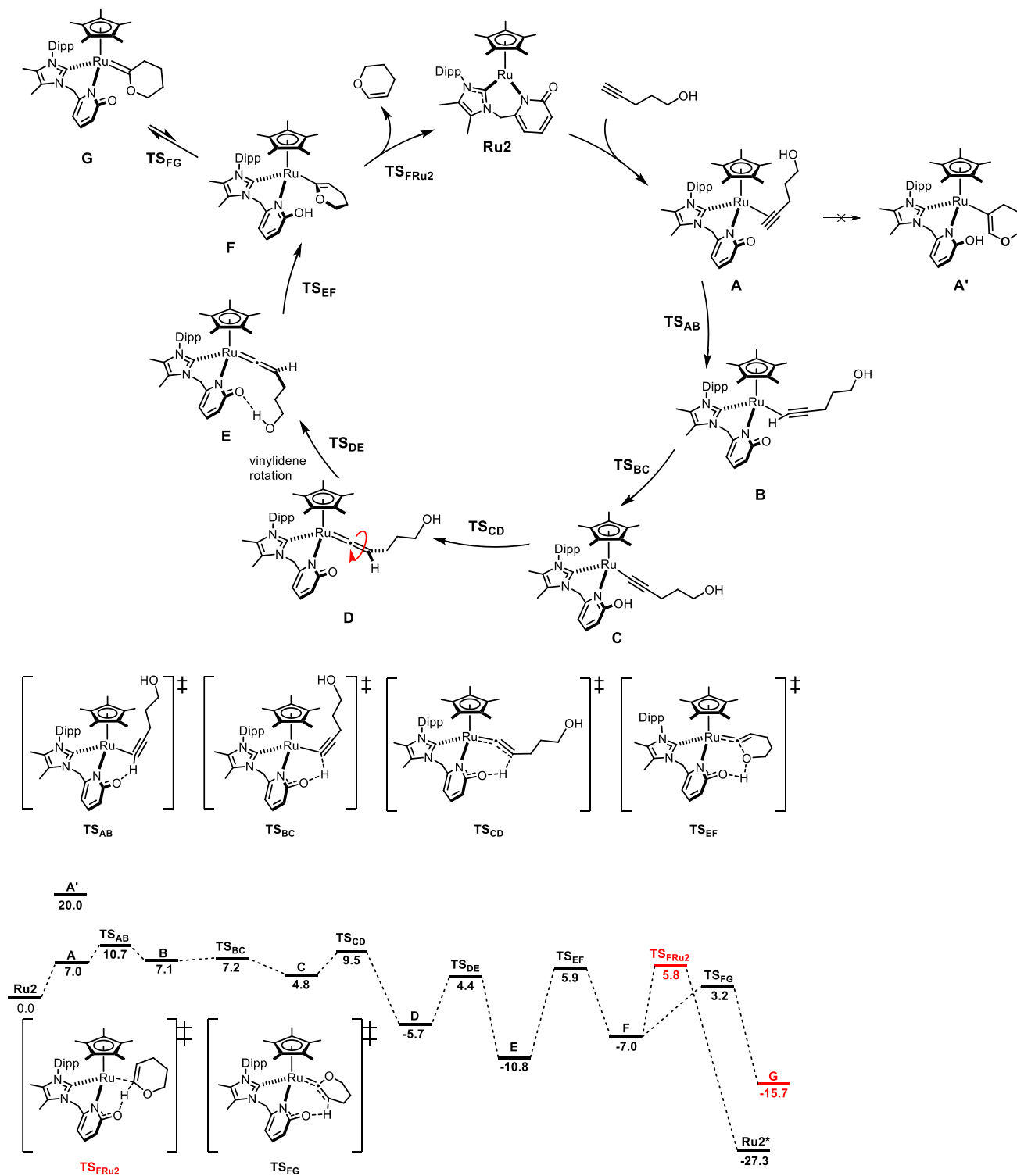


Figure 4. Computed reaction mechanism. Catalytic cycle (top) and Gibbs free energy profile in kcal mol⁻¹ at 298 K and transition state structures (bottom) of **Ru2**-catalyzed cycloisomerization of 4-pentyn-1-ol (see the Supporting Information for computation details).

is that the presence of the aromatic ring adjacent to the alkyne group makes the Ru-alkynyl intermediate more stable than the free starting materials. Secondly, the conjugation makes the ring closure step more facile and exergonic. The stable ring closed intermediate **M** (Figure S166), in turn, makes the product-releasing more facile since an early transition state is involved (transition state free energy: 5.8 kcal mol⁻¹ (for **C10**) vs -2.6 kcal mol⁻¹ (for **C3**)). Although the formation of a

stable off-cycle alkoxy carbene species **N** (Figure S166) is still faster than product release, the energy difference between **M** and **N** is smaller (4.8 kcal mol⁻¹ as opposed to 8.7 kcal mol⁻¹ between **F** and **G**) due to the disruption of the π -system in **M**. The energetic span of the overall reaction is only 16.2 kcal mol⁻¹ (between **N** and **TS_MRu2** in Figure S166).

The role of the Ru-alkoxy carbene complex has been debated in the literature,^{36,72,73} i.e., key intermediate vs off-cycle

species, especially for the catalytic formation of **C11**. Therefore, we computed the energetics of the cycloisomerization reaction of 3-butyn-1-ol catalyzed by **Ru1**, which takes 10 h at 80 °C to reach completion (Table 1). Similar to the pathway in Figure 4, the formation of the ring closed intermediate **T** from **Ru1** and 3-butyn-1-ol is facile (i.e., the free energy barrier is 14.4 kcal mol⁻¹ between **S** and **TS_{Sr}** in Figure S167); the product-releasing step has a higher barrier than the formation of the off-cycle Ru-alkoxycarbene species **RuOx** (Figure S167). The free energy span is 25.1 kcal mol⁻¹, consistent with the observed slow turnovers.

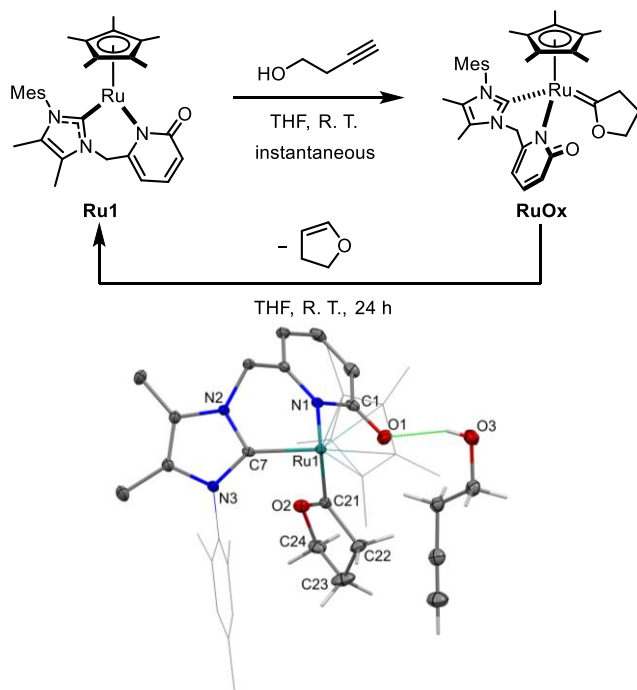


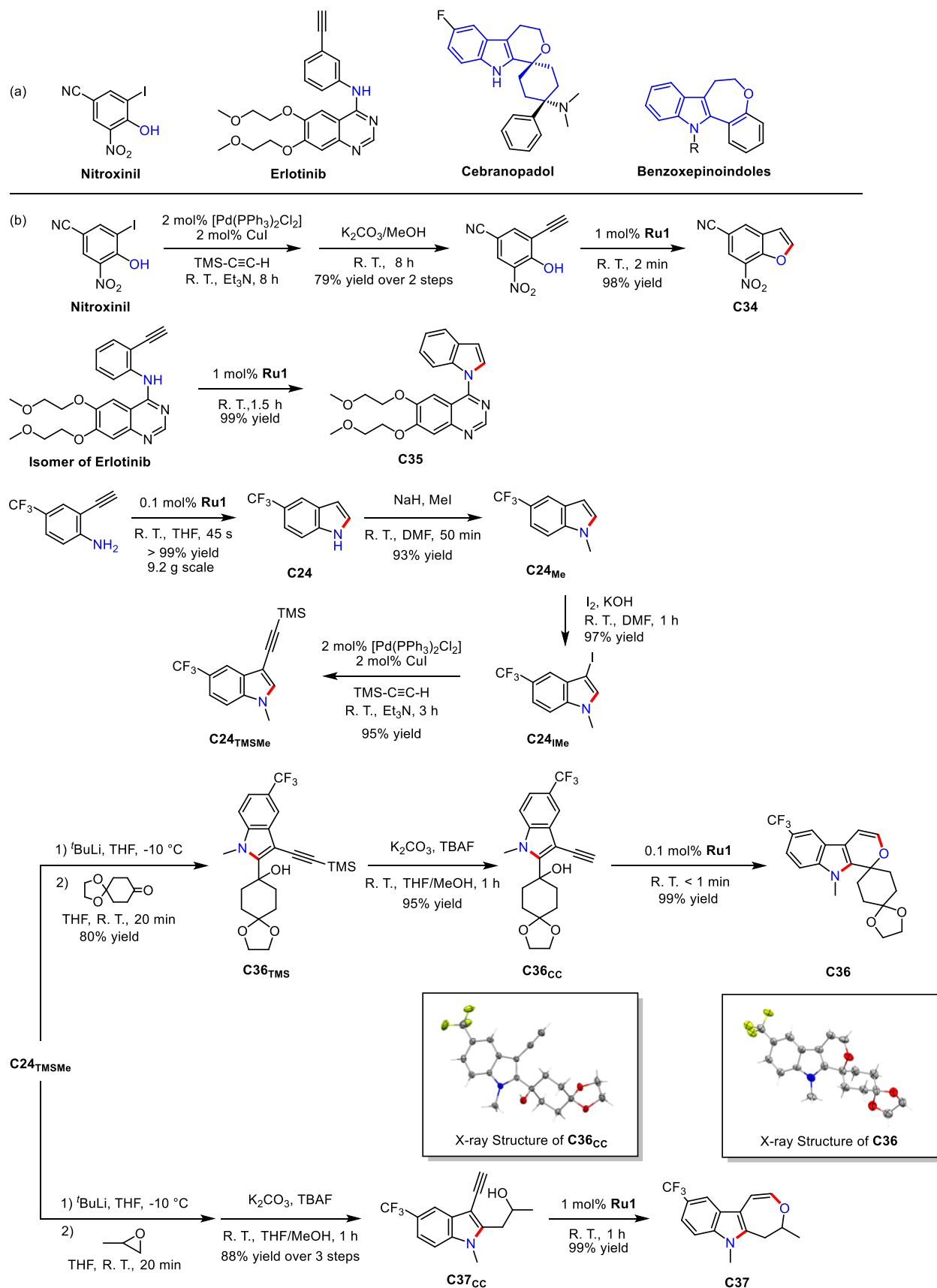
Figure 5. Synthesis of **RuOx** and product release from **RuOx** (top) and X-ray structure of **RuOx** hydrogen-bonded to 3-butyn-1-ol (bottom).

The computed energetics suggest that **RuOx** should be isolable from the reaction of **Ru1** with 3-butyn-1-ol at room temperature. Indeed, when **Ru1** is reacted with 4 equiv. of 3-butyn-1-ol, the formation of **RuOx** is instantaneous at room temperature (Figure 5) with a marked color change from purple to yellow. The immediate work-up and crystallization at -35 °C gives a crystalline sample of **RuOx** suitable for X-ray crystallography in a 72% yield. As shown in Figure 5, **RuOx** co-crystallized with one equiv. of 3-butyn-1-ol hydrogen-bonded to the pyridone oxygen with the O1–O3 distance of ~2.6 Å, typical for a strong hydrogen bond. Such a strong hydrogen bond may be relevant to the inhibition of catalysis by excess substrate or added alcohol observed in the kinetic experiments (Figure 3a). The C–C bonds (C21–C22, C22–C23, and C23–C24) within the alkoxy carbene ligand display typical single bond lengths. The Ru1–C21 bond length is 1.953(3) Å, showing a partial double bond character, shorter than the Ru1–C7 bond (2.036(3) Å). The O2–C21 (1.331(2) Å) is significantly shorter than O2–C24 bond (1.495(3) Å), suggesting a partial π -bond between the oxygen and carbene carbon. In the ¹H NMR spectrum recorded in C₆D₆, all the protons of the cyclic alkoxy carbene ligand in **RuOx** give unique signals, indicative of a rigid unsymmetrical environment. In the ¹³C NMR spectrum, the carbene carbon of

the NHC resonates at 193.7 ppm, whereas that of the cyclic alkoxy carbene ligand at 285.5 ppm, slightly more upfield compared to the literature values.⁶¹ Complex **RuOx** is unstable in solution and decomposes slowly but cleanly into 2,3-dihydrofuran and **Ru1** within 24 h at room temperature in THF or C₆D₆. The related Ru-alkoxy carbene species in the literature are either stuck to the metal center or require forcing conditions in the presence of an external base to release 2,3-dihydrofuran.^{36,72,73}

To further explore the applicability of the **Ru1** catalytic system, the syntheses of several drug derivatives/analogues were targeted (Scheme 3). The alkyne-functionalized Nitroxinil can be cyclized cleanly into **C34** within minutes at room temperature at 1 mol% catalyst loading. The cyclization of the *ortho*-isomer of Erlotinib results in the quantitative formation of **C35** within 1.5 h under the same conditions, demonstrating the feasibility of using a secondary amine nucleophile in the presence of the coordinating quinazoline and chelating ether functional groups. These two derivatives exemplify the ease of modification of existing bioactive molecules and further expand the functional group tolerance to the nitro group and quinazoline moieties.

The pyranindole moiety has found use in many pharmaceuticals including antiinflammatory⁷⁴ and antibacterial⁷⁵ drugs. Many synthetic methods have been developed for pyranindoles and other indole-containing polycyclic compounds^{76,77} including those involving transition metal catalysts;^{78–80} however, to the best of our knowledge, no single catalytic system has been used to construct both the indole and pyran rings in the fused system, not to mention being able to do so under mild conditions. We set to build the pyrano[3,4-*b*]indole core in Cebranopadol using our catalytic method (Scheme 3). The synthetic route begins with a large-scale (9.20 g) synthesis of indole **C24** using 0.1 mol% loading of **Ru1**, which reaches completion within 45 s at room temperature. The exothermic character of the reaction is evident at this scale as the reaction mixture starts boiling on its own. *N*-Methylation of **C24** followed by iodination with I₂ gives 3-iodo-*N*-methyl intermediate **C24_{IMe}**, which is then subjected to a Sonogashira coupling to install the alkyne moiety at the 3-position to give **C24_{TMSMe}**. Lithiation of **C24_{TMSMe}** at the 2-position furnishes intermediate **C36_{TMS}** after quenching with 1,4-cyclohexanedione monoethylene acetal. The removal of TMS group of **C36_{TMS}** gives intermediate **C36_{CC}**, whose solid-state structure was confirmed by X-ray crystallography. Cyclization of **C36_{CC}** with 0.1 mol% of **Ru1** on a preparative scale (200 mg) furnishes the target compound **C36** in 99% yield in 5 s at room temperature. Low-quality single crystals of **C36** were obtained and subjected to X-ray crystallographic analysis to confirm the solid-state structure. The synthetic route can be easily diverged toward a different fused ring system by reacting lithiated **C24_{TMSMe}** with other electrophiles. For example, quenching of lithiated **C24_{TMSMe}** with propylene oxide, followed by deprotection and our catalytic cyclization, affords a rare oxepino[4,5-*b*]indole compound **C37**, whose skeleton appears in a family of bioactive benzoxepinoindoles. The lithiation of **C24_{TMSMe}** can also proceed at room temperature albeit with a slightly lower yield, which renders the entire synthetic protocol achievable in just a few hours exclusively at room temperature. Additionally, the protocol can be modified to access other regioisomeric oxepino- or pyranindoles.



Scheme 3. Synthetic applications of Ru1-catalyzed cycloisomerization: (a) A few selected drug and bioactive molecules; (b) Applications of Ru1 toward the syntheses of molecules that are derivatives or analogues of molecules in (a).

CONCLUSION

We have synthesized two new charge-neutral and coordinatively unsaturated piano-stool ruthenium catalysts, **Ru1** and **Ru2**, bearing *C,N*-chelate ligands, in which the dangling pyridone oxygen atom is positioned adjacent to the substrate binding site. The participation of the pyridone oxygen plays a key role in various proton-shuttling steps of the catalytic cycloisomerization reactions, e.g., the formation of alkynyl and vinylidene intermediates, the ring closure, and the product release. Terminal alkynes functionalized with a large variety of nucleophiles (e.g., *O*-, *N*-, and *S*-based) can be cyclized without additives; most reactions can be performed at room temperature with low catalyst loadings. The cycloisomerization of aliphatic alkynols is challenging due to the formation of stable off-cycle alkoxy-carbene complexes via the preferential proton transfer to the C_{β} of the vinyl intermediate. The presence of an aromatic ring in conjugation with the alkyne moiety makes the reaction more facile by stabilizing the product release transition state via conjugation. Closing large aliphatic rings without an adjacent aromatic system is still a challenge (e.g., **C18**), as it is presumably entropically disfavored in addition to the formation of stable off-cycle alkoxy-carbene species. We further demonstrated the utility and scalability of our catalytic system toward the derivatization of drug or analogue and the syntheses of pyrano[3,4-*b*]indole and oxepino[4,5-*b*]indole structural motifs from a simple commercially available aniline, where multiple rings in the fused systems can be constructed using **Ru1**. In the synthesis of **C36**, we demonstrated that the catalyst loading can be further reduced to 0.1 mol% and the reaction reaches completion in five seconds, which translates to an average turnover frequency of 200 s⁻¹ over the course of the reaction. To the best of our knowledge, **Ru1** is the most active catalyst for such transformations to date.

METHODS AND MATERIALS

General Remarks Unless otherwise stated all reactions were carried out in a dinitrogen-filled glovebox or using standard Schlenk techniques under a dinitrogen atmosphere. The glassware was dried in a 180 °C oven overnight prior to use. Diethyl ether, hexanes, *n*-pentane, and toluene solvents were dried by refluxing and distilling over sodium under dinitrogen. THF solvent was dried by refluxing and distilling over sodium benzophenone ketyl under dinitrogen. C₆D₆ and THF-*d*₈ were degassed through three consecutive freeze-pump-thaw cycles. All solvents were stored over 3 Å molecular sieves overnight prior to use. Unless otherwise noted, all chemicals were purchased from commercial sources and used as received. All purchased liquid substrates were distilled over CaH₂ and stored over 3 Å molecular sieves overnight prior to catalysis. Complexes **RuIMes**⁷⁰ and **RuCycNHC**⁵⁸ were synthesized according to known procedures. All NMR spectra were recorded at 25 °C on an Agilent DD2 600 MHz Spectrometer, an Agilent DD2 500 MHz Spectrometer with a ¹³C-sensitive cryogenically cooled probe or a Dual Resonance (OneNMR) and Triple Resonance (HFX) probes or an Agilent VnmrS 400 MHz Spectrometer. Chemical shifts are referenced to the residual protic solvent signals unless stated otherwise and NMR signal assignments were made using 2D NMR experiments. Elemental analyses were carried out at the ANALEST of the University of Toronto. Low-resolution mass spectrometry data was obtained using an Agilent 7890A GC

System equipped with an Agilent 5975C inert XL MS detector. High resolution ESI-MS data were obtained on a ThermoFisher Scientific Q Exactive Orbitrap mass spectrometer. High-resolution mass spectrometry with DART ion source was performed using a JEOL AccuTOF Plus 4G.

General Synthetic Method for the Proligand Salts A suspension of 2-(chloromethyl)pyridin-2(1*H*)-one (1 eq.) and an appropriate imidazole⁸¹ (1.2 eq.) in MeCN (15 mL/g of pyridone) was refluxed in air for 48 h. After the removal of all volatiles by vacuum, the remaining gum was sonicated with ether to yield the crude compound as a powder.

L1•H₂Cl: Off-white crystalline solid after recrystallization from hot acetone. X-ray-quality single crystals were grown by top layering a saturated solution of the compound in acetone with Et₂O at room temperature (2.99 g, Yield = 60%, 14.0 mmol pyridone scale).

¹H NMR: (600 MHz, CDCl₃) δ 10.07 (s, 1H, procarbenic imz -CH), 7.30 (dd, *J* = 9.2, 6.7 Hz, 1H, py β-CH), 6.94 (s, 2H, Mes -CH), 6.47 (d, *J* = 6.8 Hz, 1H, py γ-CH), 6.42 (d, *J* = 9.0 Hz, 1H, py α-CH), 5.88 (s, 2H, -CH₂-), 2.38 (s, 3H, py side imz -CH₃), 2.29 (s, 3H, Mes *p*-CH₃), 1.93 (s, 6H, Mes *o*-CH₃), 1.86 (s, 3H, Mes side imz -CH₃); ¹³C NMR: (126 MHz, CDCl₃) δ 164.2 (-C=O), 141.2 (Mes *o*-C), 141.0 (py δ-C), 140.8 (py β-C), 137.2 (procarbenic imz -C), 134.9 (Mes *p*-C), 129.8 (Mes *m*-C), 129.0 (Mes *ipso*-C), 128.2 (py side imz -C), 127.3 (Mes side imz -C), 120.5 (py α-C), 108.0 (py γ-C), 48.0 (-CH₂-), 21.2 (Mes *p*-CH₃), 17.6 (Mes *o*-CH₃), 9.6 (py side imz -CH₃), 8.2 (Mes side imz -CH₃); HRMS (ESI⁺): *m/z* calc'd for C₂₀H₂₄N₃O⁺ [M-Cl⁺]: 322.1914; found: 322.1909.

L2•H₂Cl: Gray powder after top layering a saturated solution of the compound in *i*-PrOH:Acetone 1:1 with Et₂O at -20 °C (3.40 g, Yield = 61%, 14.0 mmol pyridone scale).

¹H NMR: (500 MHz, CDCl₃) δ 12.64 (br. s, 1H, N-H), 10.40 (s, 1H, procarbenic imz -CH), 7.52 (t, *J* = 7.8 Hz, 1H, Dipp *p*-CH), 7.33 (dd, *J* = 9.2, 6.7 Hz, 1H, py β-CH), 7.28 (d, *J* = 7.8 Hz, 2H, Dipp *m*-CH), 6.56 – 6.45 (app. m, 2H, py α and γ-CH), 5.98 (s, 2H, -CH₂-), 2.47 (s, 3H, py side imz -CH₃), 2.15 (hept, *J* = 6.8 Hz, 2H, Dipp ^{*i*}Pr -CH-), 1.90 (s, 3H, Dipp side imz -CH₃), 1.13 (dd, *J* = 6.8, 3.7 Hz, 12H, Dipp ^{*i*}Pr -CH₃); ¹³C NMR: (126 MHz, CDCl₃) δ 164.1 (-C=O), 145.8 (Dipp *o*-C), 141.3 (py δ-C), 140.9 (py β-C), 137.7 (procarbenic imz -C), 131.9 (Dipp *p*-C), 128.3 (Dipp *ipso*-C), 128.1 (Dipp and py side imz -C), 124.9 (Dipp *m*-C), 120.7 (py α-C), 107.9 (py γ-C), 47.9 (-CH₂-), 28.7 (Dipp ^{*i*}Pr -CH-), 25.1 (Dipp ^{*i*}Pr -CH₃), 23.1 (Dipp ^{*i*}Pr -CH₃), 9.7 (py side imz -CH₃), 8.6 (Dipp side imz -CH₃); HRMS (ESI⁺): *m/z* calc'd for C₂₃H₃₀N₃O⁺ [M-Cl⁺]: 364.2383; found: 364.2377.

General Synthetic Method for the Ru Complexes To a 20 mL scintillation vial were added imidazolium salt (1.0 mmol, 1 eq), potassium *tert*-butoxide (224 mg, 2.0 mmol, 2 eq) and cold THF (15 mL, -35 °C). The resulting suspension was stirred at -35 °C for 1 h. The now clear solution was added to a suspension of [Cp**Ru*Cl]₄⁸² (272 mg, 0.25 mmol, 0.25 eq.) in THF (5 mL) at room temperature turning deep purple in color instantly. The mixture was stirred at room temperature for 4 h, filtered through a pad of Celite and evaporated to dryness under reduced pressure. The resulting solids were washed with cold Et₂O (2 × 5 mL, -35 °C) and *n*-pentane (2 × 5 mL) to yield the crude products.

Ru1: X-ray-quality bluish-purple crystals after recrystallization by vapor diffusion of *n*-pentane into a concentrated solu-

tion of the complex in THF at room temperature after 12 h. The supernatant was discarded, and the crystals washed with Et₂O (5 mL) and *n*-pentane (5 mL) and dried under vacuum. (500 mg, Yield = 90%).

¹H NMR: (600 MHz, C₆D₆) δ 7.11 (dd, *J* = 8.7, 6.4 Hz, 1H, py β-CH), 6.82 (s, 1H, outward-facing Mes -CH), 6.69 (s, 1H, Ru-facing Mes -CH), 6.64 (d, *J* = 8.7, 1H, py α-CH), 5.91 (d, *J* = 6.4, 1H, py γ-CH), 4.27 (d, *J* = 13.5 Hz, 1H, Cp*-facing -CH₂-), 4.23 (d, *J* = 13.5 Hz, 1H, outward-facing -CH₂-), 2.14 (s, 3H, outward-facing Mes *o*-CH₃), 2.11 (s, 3H, Mes *p*-CH₃), 1.59 (s, 3H, py side imz -CH₃), 1.52 (s, 15H, Cp*-CH₃), 1.43 (s, 3H, Mes side imz -CH₃), 1.17 (s, 3H, Ru-facing Mes *o*-CH₃); **¹³C NMR:** (126 MHz, C₆D₆) δ 199.9 (carbene imz -C), 170.2 (-C=O), 150.3 (py δ-C), 138.6 (Ru-facing Mes *o*-C), 137.7 (Mes *p*-C), 136.3 (py β-C), 136.1 (Mes *ipso*-C), 134.4 (outward-facing Mes *o*-C), 130.2 (Ru-facing Mes *m*-C), 128.7 (outward-facing Mes *m*-C), 125.6 (Mes side imz -C), 123.2 (py side imz -C), 116.2 (py α-C), 102.4 (py γ-C), 76.4 (Cp* η-C), 52.5 (-CH₂-), 21.0 (Mes *p*-CH₃), 18.4 (outward-facing Mes *o*-CH₃), 18.2 (Ru-facing Mes *o*-CH₃), 11.6 (Cp*-CH₃), 9.0 (Mes side imz -CH₃), 8.7 (py side imz -CH₃); Anal. calc'd for C₃₀H₃₇N₃ORu: C 64.72, H 6.70, N 7.55; found: C 64.63, H 6.58, N 7.41.

Ru2: Purple microcrystals after recrystallization by vapor diffusion of *n*-pentane into a concentrated solution of the complex in THF at -35 °C after 5 days. The supernatant was discarded, and the crystals were washed with *n*-pentane (5 mL) and dried under vacuum. X-ray-quality crystals were obtained by vapor diffusion of *n*-pentane into a diluted solution of the complex in THF at -35 °C (584 mg, Yield = 98%).

¹H NMR: (500 MHz, C₆D₆) δ 7.21–7.19 (m, 1H, Dipp *p*-CH), 7.18–7.14 (m, 2H, Dipp *m*-CH), 7.10 (dd, *J* = 8.8, 6.4 Hz, 1H, py β-CH), 6.68 (d, *J* = 8.7, 1H, py α-CH), 5.87 (d, *J* = 6.4 Hz, 1H, py γ-CH), 4.40 (d, *J* = 13.6, 1H, Cp*-facing -CH₂-), 4.24 (d, *J* = 13.5 Hz, 1H, outward-facing -CH₂-), 3.02 (hept, *J* = 6.8 Hz, 1H, outward-facing Dipp ⁱPr -CH-), 1.60 (s, 3H, py side imz -CH₃), 1.53 (s, 15H, Cp*-CH₃), 1.46 (s, 3H, Dipp side imz -CH₃), 1.33 (d, *J* = 6.8 Hz, 3H, outward-facing Dipp ⁱPr -CH₃), 1.20 (d, *J* = 6.6 Hz, 3H, Ru-facing Dipp ⁱPr -CH₃), 1.16 (d, *J* = 6.7 Hz, 3H, outward-facing Dipp ⁱPr -CH₃), 0.28 (d, *J* = 6.7 Hz, 3H, Ru-facing Dipp ⁱPr -CH₃), 0.08 (hept, *J* = 6.6 Hz, 1H, Ru-facing Dipp ⁱPr -CH-); **¹³C NMR:** (126 MHz, C₆D₆) δ 200.4 (carbene imz -C), 170.5 (-C=O), 150.4 (py δ-C), 147.9 (Ru-facing Dipp *o*-C), 145.4 (outward-facing Dipp *o*-C), 136.2 (py β-C and Dipp *ipso*-C), 129.1 (Dipp *p*-C), 127.1 (Dipp side imz -C), 124.7 (Ru-facing Dipp *m*-C), 124.1 (outward-facing Dipp *m*-C), 123.6 (py side imz -C), 116.7 (py α-C), 102.3 (py γ-C), 75.4 (Cp* η-C), 53.1 (-CH₂-), 29.8 (Ru-facing Dipp ⁱPr -CH-), 28.2 (outward-facing Dipp ⁱPr -CH-), 25.4 (outward-facing Dipp ⁱPr -CH₃), 24.7 (Ru-facing Dipp ⁱPr -CH₃), 24.6 (outward-facing Dipp ⁱPr -CH₃), 21.7 (Ru-facing Dipp ⁱPr -CH₃), 11.7 (Cp*-CH₃), 10.1 (Dipp side imz -CH₃), 8.8 (py side imz -CH₃); Anal. calc'd for C₃₃H₄₃N₃ORu: C 66.19, H 7.24, N 7.02; found: C 66.07, H 7.46, N 6.74.

General Procedure for the Catalytic Runs Stock solutions of the catalysts at the concentrations of 12.0 mmol L⁻¹, 4.0 mmol L⁻¹ and 0.4 mmol L⁻¹ in THF were prepared. In a dinitrogen-filled glovebox, a 1 dram vial was charged with substrate (0.20 mmol), mesitylene (0.20 mmol) as internal standard, and a stir bar. The catalyst stock solution (0.5 mL) was then added, and the mixture was stirred at the desired temperature for the required time measured using a chronometer. The

fast catalytic trials, which finish either instantly or within 5–50 s, are all described as complete in < 1 min, while the slow trials were followed by TLC until completion. The reaction vessel was cooled to room temperature first if higher temperatures were used and opened to the ambient atmosphere to quench the catalyst. A 0.1 mL aliquot of the mixture was diluted with 0.4 mL of CDCl₃, filtered through glass fiber, and taken to the NMR spectrometer for analysis. Acquisition parameters were selected to allow for maximum relaxation of the nuclei for accurate quantitation (16 scans with 25 s relaxation delay and 90° pulse angle).

AUTHOR INFORMATION

Corresponding Author

*Datong Song d.song@utoronto.ca

ASSOCIATED CONTENT

Supporting Information.

This material is available free of charge via the Internet at <http://pubs.acs.org>

Additional experimental procedures, NMR and IR spectra, selected X-ray crystallographic data, and computation details.

Accession Codes

CCDC 2304666–2304674, 2345323, and 2345324 contain the supplementary crystallographic data for this paper. These data can be obtained free of charge via www.ccdc.cam.ac.uk/data_request/cif, or by emailing data_request@ccdc.cam.ac.uk, or by contacting The Cambridge Crystallographic Data Centre, 12 Union Road, Cambridge CB2 1EZ, UK; fax: +44 1223 336033.

ACKNOWLEDGMENTS

We thank the Natural Sciences and Engineering Research Council (NSERC) of Canada for a Discovery Grant (RGPIN-2019-06576). We also acknowledge the Canadian Foundation for Innovation Project #19119. H.A.G.M. thanks the Mexican National Council for Science and Technology (CONACyT) for a graduate fellowship. This research was enabled in part by support provided by Shared Hierarchical Academic Research Computing Network (SHARCNET) (www.sharcnet.ca) and Digital Research Alliance of Canada (alliancecan.ca).

REFERENCES

- (1) Pozharskii, A. F.; Soldatenkov, A. T.; Katritzky, A. R. *Heterocycles in Life and Society: An Introduction to Heterocyclic Chemistry, Biochemistry and Applications*, 1st ed., Wiley, 2011.
- (2) Heravi, M. M.; Zadsirjan, V. Prescribed Drugs Containing Nitrogen Heterocycles: An Overview. *RSC Adv.* **2020**, *10*, 44247–44311.
- (3) Vitaku, E.; Smith, D. T.; Njardarson, J. T. Analysis of the Structural Diversity, Substitution Patterns, and Frequency of Nitrogen Heterocycles among U.S. FDA Approved Pharmaceuticals: Miniperspective. *J. Med. Chem.* **2014**, *57*, 10257–10274.
- (4) Delost, M. D.; Smith, D. T.; Anderson, B. J.; Njardarson, J. T. From Oxiranes to Oligomers: Architectures of U.S. FDA Approved Pharmaceuticals Containing Oxygen Heterocycles. *J. Med. Chem.* **2018**, *61*, 10996–11020.
- (5) Patil, N. T.; Yamamoto, Y. Coinage Metal-Assisted Synthesis of Heterocycles. *Chem. Rev.* **2008**, *108*, 3395–3442.

- (6) Trost, B. M.; McClory, A. Metal Vinylidenes as Catalytic Species in Organic Reactions. *Chem. Asian J.* **2008**, *3*, 164–194.
- (7) Roh, S. W.; Choi, K.; Lee, C. Transition Metal Vinylidene- and Allenylidene-Mediated Catalysis in Organic Synthesis. *Chem. Rev.* **2019**, *119*, 4293–4356.
- (8) Varela, J. A.; González-Rodríguez, C.; Saá, C. Catalytic Transformations of Alkynes via Ruthenium Vinylidene and Allenylidene Intermediates. In *Ruthenium in Catalysis*; Dixneuf, P. H., Bruneau, C., Eds.; Topics in Organometallic Chemistry; Springer International Publishing: Cham, 2014; Vol. 48, pp 237–287.
- (9) McDonald, F. E.; Connolly, C. B.; Gleason, M. M.; Towne, T. B.; Treiber, K. D. A New Synthesis of 2,3-Dihydrofurans: Cycloisomerization of Alkynyl Alcohols to Endocyclic Enol Ethers. *J. Org. Chem.* **1993**, *58*, 6952–6953.
- (10) McDonald, F. E.; Schultz, C. C. Mechanism of Molybdenum Pentacarbonyl-Catalyzed Cyclizations of Alkynols and Epoxyalkynes. *J. Am. Chem. Soc.* **1994**, *116*, 9363–9364.
- (11) Dorel, R.; Echavarren, A. M. Gold(I)-Catalyzed Activation of Alkynes for the Construction of Molecular Complexity. *Chem. Rev.* **2015**, *115*, 9028–9072.
- (12) Praveen, C. Cycloisomerization of π -Coupled Heteroatom Nucleophiles by Gold Catalysis: En Route to Regiochemically Defined Heterocycles. *Chem. Rec.* **2021**, *21*, 1697–1737.
- (13) McDonald, F. E.; Reddy, K. S.; Díaz, Y. Stereoselective Glycosylations of a Family of 6-Deoxy-1,2-Glycals Generated by Catalytic Alkynol Cycloisomerization. *J. Am. Chem. Soc.* **2000**, *122*, 4304–4309.
- (14) McDonald, F. E.; Reddy, K. S. Convergent Synthesis of Digitoxin: Stereoselective Synthesis and Glycosylation of the Digoxin Trisaccharide Glycal. *Angew. Chem. Int. Ed.* **2001**, *40*, 3653–3655.
- (15) McDonald, F. E.; Gleason, M. M. Asymmetric Syntheses of Stavudine (d4T) and Cordycepin by Cycloisomerization of Alkynyl Alcohols to Endocyclic Enol Ethers. *Angew. Chem. Int. Ed. Engl.* **1995**, *34*, 350–352.
- (16) McDonald, F. E.; Gleason, M. M. Asymmetric Synthesis of Nucleosides via Molybdenum-Catalyzed Alkynol Cycloisomerization Coupled with Stereoselective Glycosylations of Deoxyfuranose Glycals and 3-Amidofuranose Glycals. *J. Am. Chem. Soc.* **1996**, *118*, 6648–6659.
- (17) Koo, B.; McDonald, F. E. Synthesis of the Branched C-Glycoside Substructure of Altromycin B. *Org. Lett.* **2005**, *7*, 3621–3624.
- (18) Koo, B.; McDonald, F. E. Fischer Carbene Catalysis of Alkynol Cycloisomerization: Application to the Synthesis of the Altromycin B Disaccharide. *Org. Lett.* **2007**, *9*, 1737–1740.
- (19) Trost, B. M.; Rhee, Y. H. A Rh(I)-Catalyzed Cycloisomerization of Homo- and Bis-Homopropargylic Alcohols. *J. Am. Chem. Soc.* **2003**, *125*, 7482–7483.
- (20) Trost, B. M.; Seganish, W. M.; Chung, C. K.; Amans, D. Total Synthesis of Laulimalide: Synthesis of the Northern and Southern Fragments. *Chem. Eur. J.* **2012**, *18*, 2948–2960.
- (21) Trost, B. M.; McClory, A. Rhodium-Catalyzed Cycloisomerization: Formation of Indoles, Benzofurans, and Enol Lactones. *Angew. Chem. Int. Ed.* **2007**, *46*, 2074–2077.
- (22) Kim, H.; Lee, C. Rhodium-Catalyzed Cycloisomerization of N-Propargyl Enamine Derivatives. *J. Am. Chem. Soc.* **2006**, *128*, 6336–6337.
- (23) Chung, L.-H.; Wong, C.-Y. Ruthenium-Induced Alkyne Cycloisomerization: Construction of Metalated Heterocycles, Revelation of Unconventional Reaction Pathways, and Exploration of Functional Applications. *Chem. Eur. J.* **2019**, *25*, 2889–2897.
- (24) Chung, L.-H.; Yeung, C.-F.; Wong, C.-Y. Ruthenium-Induced Cyclization of Heteroatom-Functionalized Alkynes: Progress, Challenges and Perspectives. *Chem. Eur. J.* **2020**, *26*, 6102–6112.
- (25) Trost, B. M.; Rhee, Y. H. A Ru Catalyzed Divergence: Oxidative Cyclization vs Cycloisomerization of Bis-Homopropargylic Alcohols. *J. Am. Chem. Soc.* **2002**, *124*, 2528–2533.
- (26) Varela-Fernández, A.; González-Rodríguez, C.; Varela, J. A.; Castedo, L.; Saá, C. Cycloisomerization of Aromatic Homo- and Bis-Homopropargylic Alcohols via Catalytic Ru Vinylidenes: Formation of Benzofurans and Isochromenes. *Org. Lett.* **2009**, *11*, 5350–5353.
- (27) Varela-Fernández, A.; Varela, J. A.; Saá, C. Formation of Indoles, Dihydroisoquinolines, and Dihydroquinolines by Ruthenium-Catalyzed Heterocyclizations. *Synthesis* **2012**, *44*, 3285–3295.
- (28) Varela-Fernández, A.; Varela, J. A.; Saá, C. Ruthenium-Catalyzed Cycloisomerization of Aromatic Homo- and Bis-Homopropargylic Amines/Amides: Formation of Indoles, Dihydroisoquinolines and Dihydroquinolines. *Adv. Synth. Catal.* **2011**, *353*, 1933–1937.
- (29) Varela-Fernández, A.; García-Yebra, C.; Varela, J. A.; Esteruelas, M. A.; Saá, C. Osmium-Catalyzed 7-Endo Heterocyclization of Aromatic Alkynols into Benzoxepines. *Angew. Chem. Int. Ed.* **2010**, *49*, 4278–4281.
- (30) Álvarez-Pérez, A.; González-Rodríguez, C.; García-Yebra, C.; Varela, J. A.; Oñate, E.; Esteruelas, M. A.; Saá, C. Catalytic Cyclization of o-Alkynyl Phenethylamines via Osmacyclopentene Intermediates: Direct Access to Dopaminergic 3-Benzazepines. *Angew. Chem. Int. Ed.* **2015**, *54*, 13357–13361.
- (31) Shelton, P. A.; Hilliard, C. R.; Swindling, M.; McElwee-White, L. Dimerization of Ethynylaniline to a Quinoline Derivative Using a Ruthenium/Gold Heterobimetallic Catalyst. *Arkivoc* **2010**, 160–166.
- (32) Grotjahn, D. B.; Lev, D. A. A General Bifunctional Catalyst for the Anti-Markovnikov Hydration of Terminal Alkynes to Aldehydes Gives Enzyme-Like Rate and Selectivity Enhancements. *J. Am. Chem. Soc.* **2004**, *126*, 12232–12233.
- (33) Nair, R. N.; Lee, P. J.; Grotjahn, D. B. One-Pot Formation of Functionalized Indole and Benzofuran Derivatives Using a Single Bifunctional Ruthenium Catalyst. *Top. Catal.* **2010**, *53*, 1045–1047.
- (34) Nair, R. N.; Lee, P. J.; Rheingold, A. L.; Grotjahn, D. B. Single Bifunctional Ruthenium Catalyst for One-Pot Cyclization and Hydration Giving Functionalized Indoles and Benzofurans. *Chem. Eur. J.* **2010**, *16*, 7992–7995.
- (35) Liu, P. N.; Su, F. H.; Wen, T. B.; Sung, H. H.-Y.; Williams, I. D.; Jia, G. Selective and Efficient Cycloisomerization of Alkynols Catalyzed by a New Ruthenium Complex with a Tetradentate Nitrogen–Phosphorus Mixed Ligand. *Chem. Eur. J.* **2010**, *16*, 7889–7897.
- (36) Cai, T.; Yang, Y.; Li, W.; Qin, W.; Wen, T. Efficient Endo Cycloisomerization of Terminal Alkynols Catalyzed by a New Ruthenium Complex with 8-(Diphenylphosphino)Quinoline Ligand and Mechanistic Investigation. *Chem. Eur. J.* **2018**, *24*, 1606–1618.

- (37) Stubbs, J. M.; J. Bridge, B.; M. Blacquiere, J. Optimizing Ligand Structure for Low-Loading and Fast Catalysis for Alkynyl-Alcohol and -Amine Cyclization. *Dalton Trans.* **2019**, *48*, 7928–7937.
- (38) Stubbs, J. M.; Chapple, D. E.; Boyle, P. D.; Blacquiere, J. M. Catalyst Pendant-Base Effects on Cyclization of Alkynyl Amines. *ChemCatChem* **2018**, *10*, 4001–4009.
- (39) Stubbs, J. M.; Bow, J.-P. J.; Hazlehurst, R. J.; Blacquiere, J. M. Catalytic Cyclization and Competitive Deactivation with Ru(P^R₂N^{R'}₂) Complexes. *Dalton Trans.* **2016**, *45*, 17100–17103.
- (40) Bridge, B. J.; Boyle, P. D.; Blacquiere, J. M. Endo-Selective Iron Catalysts for Intramolecular Alkyne Hydrofunctionalization. *Organometallics* **2020**, *39*, 2570–2574.
- (41) Hayashi, K.; Liang, Q.; Philippi, F.; Song, D. Piano-Stool Ruthenium N-Heterocyclic Carbene Complexes for Gem-Specific Catalytic Dimerization of Terminal Alkynes. *Eur. J. Inorg. Chem.* **2023**, *26*, e202300168.
- (42) Liang, Q.; Sheng, K.; Salmon, A.; Zhou, V. Y.; Song, D. Active Iron(II) Catalysts toward Gem -Specific Dimerization of Terminal Alkynes. *ACS Catal.* **2019**, *9*, 810–818.
- (43) Liang, Q.; Hayashi, K.; Rabeda, K.; Jimenez-Santiago, J. L.; Song, D. Piano-Stool Iron Complexes as Precatalysts for Gem -Specific Dimerization of Terminal Alkynes. *Organometallics* **2020**, *39*, 2320–2326.
- (44) Liang, Q.; Osten, K. M.; Song, D. Iron-Catalyzed Gem -Specific Dimerization of Terminal Alkynes. *Angew. Chem. Int. Ed.* **2017**, *56*, 6317–6320.
- (45) Angelis, F. D.; Sgamellotti, A.; Re, N. Acetylene to Vinylidene Rearrangements on Electron Rich D6 Metal Centers: A Density Functional Study. *Dalton Trans.* **2004**, 3225–3230.
- (46) Wakatsuki, Y. Mechanistic Aspects Regarding the Formation of Metal Vinylidenes from Alkynes and Related Reactions. *J. Organomet. Chem.* **2004**, *689*, 4092–4109.
- (47) Forlani, L.; Cristoni, G.; Boga, C.; Todesco, P. E.; Vecchio, E. D.; Selva, S.; Monari, M. Reinvestigation of the Tautomerism of Some Substituted 2-Hydroxypyridines. *Arkivoc* **2002**, *2002*, 198–215.
- (48) Rawson, J. M.; Winpenny, R. E. P. The Coordination Chemistry of 2-Pyridone and Its Derivatives. *Coord. Chem. Rev.* **1995**, *139*, 313–374.
- (49) Fujita, K.; Tanino, N.; Yamaguchi, R. Ligand-Promoted Dehydrogenation of Alcohols Catalyzed by Cp*Ir Complexes. A New Catalytic System for Oxidant-Free Oxidation of Alcohols. *Org. Lett.* **2007**, *9*, 109–111.
- (50) Wang, W.-H.; Hull, J. F.; Muckerman, J. T.; Fujita, E.; Himeda, Y. Second-Coordination-Sphere and Electronic Effects Enhance Iridium(III)-Catalyzed Homogeneous Hydrogenation of Carbon Dioxide in Water near Ambient Temperature and Pressure. *Energy Environ. Sci.* **2012**, *5*, 7923–7926.
- (51) Fujita, K.; Kawahara, R.; Aikawa, T.; Yamaguchi, R. Hydrogen Production from a Methanol–Water Solution Catalyzed by an Anionic Iridium Complex Bearing a Functional Bipyridonate Ligand under Weakly Basic Conditions. *Angew. Chem. Int. Ed.* **2015**, *54*, 9057–9060.
- (52) Iguchi, M.; Zhong, H.; Himeda, Y.; Kawanami, H. Effect of the Ortho-Hydroxyl Groups on a Bipyridine Ligand of Iridium Complexes for the High-Pressure Gas Generation from the Catalytic Decomposition of Formic Acid. *Chem. Eur. J.* **2017**, *23*, 17788–17793.
- (53) Geri, J. B.; Szymczak, N. K. A Proton-Switchable Bifunctional Ruthenium Complex That Catalyzes Nitrate Hydroboration. *J. Am. Chem. Soc.* **2015**, *137*, 12808–12814.
- (54) Afandiyeva, M.; Kadam, A. A.; Wu, X.; Brennessel, W. W.; Kennedy, C. R. Synthesis, Structure, and Hydroboration Reactivity of Anionic Nickel(0) Complexes Supported by Bidentate NHC-Pyridone Ligands. *Organometallics* **2022**, *41*, 3014–3023.
- (55) Zhuang, X.; Chen, J.-Y.; Yang, Z.; Jia, M.; Wu, C.; Liao, R.-Z.; Tung, C.-H.; Wang, W. Sequential Transformation of Terminal Alkynes to 1,3-Dienes by a Cooperative Cobalt Pyridonate Catalyst. *Organometallics* **2019**, *38*, 3752–3759.
- (56) Hasenbeck, M.; Müller, T.; Gellrich, U. Metal-Free Gem Selective Dimerization of Terminal Alkynes Catalyzed by a Pyridonate Borane Complex. *Catal. Sci. Technol.* **2019**, *9*, 2438–2444.
- (57) Galiana-Cameo, M.; Urriolabeitia, A.; Barrenas, E.; Passarelli, V.; Pérez-Torrente, J. J.; Di Giuseppe, A.; Polo, V.; Castarlenas, R. Metal–Ligand Cooperative Proton Transfer as an Efficient Trigger for Rhodium-NHC-Pyridonate Catalyzed Gem-Specific Alkyne Dimerization. *ACS Catal.* **2021**, *11*, 7553–7567.
- (58) Liang, Q.; Song, D. Reactivity of Fe and Ru Complexes of Picolyl-Substituted N-Heterocyclic Carbene Ligand: Diverse Coordination Modes and Small Molecule Binding. *Inorg. Chem.* **2017**, *56*, 11956–11970.
- (59) Tan, R.; Song, D. Interconversion between the Enantiomers of Chiral Five-Coordinate Me₃Pt(IV) Complexes. *Inorg. Chem.* **2011**, *50*, 10614–10622.
- (60) Faller, J. W. Dynamic NMR Spectroscopy in Organometallic Chemistry. In *Comprehensive Organometallic Chemistry III*; Mingos, D. M. P., Crabtree, R. H., Eds.; Elsevier: Oxford, 2007, Vol. 1, pp 407–427.
- (61) Welby, C. E.; Eschemann, T. O.; Unsworth, C. A.; Smith, E. J.; Thatcher, R. J.; Whitwood, A. C.; Lynam, J. M. Ruthenium Acetate Complexes as Versatile Probes of Metal–Ligand Interactions: Insight into the Ligand Effects of Vinylidene, Carbene, Carbonyl, Nitrosyl and Isocyanide. *Eur. J. Inorg. Chem.* **2012**, *2012*, 1493–1506.
- (62) Katayama, H.; Wada, C.; Taniguchi, K.; Ozawa, F. Effect of Substituents on the Formation of Vinylideneruthenium(II) Complexes. X-Ray Structures of RuCl₂{CC(Z)Ph}(Dcpmp) (Z = H, SiMe₃; Dcpmp = C₅H₅N(CH₂PCy₂)₂). *Organometallics* **2002**, *21*, 3285–3291.
- (63) Opstal, T.; Verpoort, F. Synthesis of Enol Esters and Dimerization of Terminal Alkynes Catalyzed by Neutral and Cationic Vinylidene Ruthenium Complexes. *Synlett* **2003**, 314–320.
- (64) Gunbas, G.; Hafezi, N.; Sheppard, W. L.; Olmstead, M. M.; Stoyanova, I. V.; Tham, F. S.; Meyer, M. P.; Mascal, M. Extreme Oxatriquinanes and a Record C–O Bond Length. *Nat. Chem.* **2012**, *4*, 1018–1023.
- (65) Bullock, R. M. Rearrangement of a Metal (η²-Alkyne) Complex to a Metal Vinylidene and Subsequent Reaction of the Metal Vinylidene to Regenerate the Alkyne. *J. Chem. Soc., Chem. Commun.* **1989**, 165–167.
- (66) Tokunaga, M.; Suzuki, T.; Koga, N.; Fukushima, T.; Horiuchi, A.; Wakatsuki, Y. Ruthenium-Catalyzed Hydration of 1-Alkynes to Give Aldehydes: Insight into a Nti -Markovnikov Regiochemistry. *J. Am. Chem. Soc.* **2001**, *123*, 11917–11924.
- (67) Grotjahn, D. B.; Miranda-Soto, V.; Kragulj, E. J.; Lev, D. A.; Erdogan, G.; Zeng, X.; Cooksy, A. L. Hydrogen-Bond Acceptance of Bifunctional Ligands in an Alkyne–Metal π Complex. *J. Am. Chem. Soc.* **2008**, *130*, 20–21.

- (68) Breit, B.; Gellrich, U.; Li, T.; Lynam, J. M.; Milner, L. M.; Pridmore, N. E.; Slattery, J. M.; Whitwood, A. C. Mechanistic Insight into the Ruthenium-Catalysed Anti-Markovnikov Hydration of Alkynes Using a Self-Assembled Complex: A Crucial Role for Ligand-Assisted Proton Shuttle Processes. *Dalton Trans.* **2014**, *43*, 11277–11285.
- (69) Benhamou, L.; Walker, D. W.; Bučar, D.-K.; Aliev, A. E.; Sheppard, T. D. Synthesis of Substituted Benzoxaborinin-1-Ols via Palladium-Catalysed Cyclisation of Alkenyl- and Alkynyl-Boronic Acids. *Org. Biomol. Chem.* **2016**, *14*, 8039–8043.
- (70) Huang, J.; Stevens, E. D.; Nolan, S. P.; Petersen, J. L. Olefin Metathesis-Active Ruthenium Complexes Bearing a Nucleophilic Carbene Ligand. *J. Am. Chem. Soc.* **1999**, *121*, 2674–2678.
- (71) McDonald, F. E.; Burova, S. A.; Huffman, L. G. Jr. Sulfur-Alkyne Cyclizations for Formation of Dihydrothiophenes and Annulated Thiophenes. *Synthesis* **2000**, *2000*, 970–974.
- (72) Chapple, D. E.; Hoffer, M. A.; Boyle, P. D.; Blacquiere, J. M. Alkyne Hydrofunctionalization Mechanism Including an Off-Cycle Alkoxy-carbene Deactivation Complex. *Organometallics* **2022**, *41*, 1532–1542.
- (73) Liu, P. N.; Wen, T. B.; Ju, K. D.; Sung, H. H.-Y.; Williams, I. D.; Jia, G. Mechanism Investigations of the Endo Cycloisomerization of Alkynols through Isolation and Characterization of Ruthenium Complexes from the Reactions of Alkynes with a Ruthenium Complex. *Organometallics* **2011**, *30*, 2571–2580.
- (74) Lynch, S.; Brogden, R. N. Etodolac: A Preliminary Review of its Pharmacodynamic Activity and Therapeutic Use. *Drugs* **1986**, *31*, 288–300.
- (75) Leboho, T. C.; Michael, J. P.; van Otterlo, W. A. L.; van Vuuren, S. F.; de Koning, C. B. The Synthesis of 2- and 3-Aryl Indoles and 1,3,4,5-Tetrahydropyrano[4,3-*b*]Indoles and Their Antibacterial and Antifungal Activity. *Bioorg. Med. Chem. Lett.* **2009**, *19*, 4948–4951.
- (76) Gao, Y.; Wang, X.; Wei, Z.; Cao, J.; Liang, D.; Lin, Y.; Duan, H. Asymmetric Synthesis of Spirooxindole–Pyranoidole Products via Friedel–Crafts Alkylation/Cyclization of the Indole Carbocyclic Ring. *New J. Chem.* **2020**, *44*, 9788–9792.
- (77) Choi, S.; Oh, H.; Sim, J.; Yu, E.; Shin, S.; Park, C.-M. Metal-Free Synthesis of Indolopyrans and 2,3-Dihydrofurans Based on Tandem Oxidative Cycloaddition. *Org. Lett.* **2020**, *22*, 5528–5534.
- (78) Kotipalli, R.; Babu, U. S.; Nanubolu, J. B.; Reddy, M. S. Rh-Catalyzed Chemo-, Stereo- and Regioselective C–H Cascade Annulation of Indolyloxopropanenitriles for Pyranoidoles. *Chem. Commun.* **2023**, *59*, 10137–10140.
- (79) Qian, J.; Sheng, G.; Huang, K.; Liu, S.; Lu, P.; Wang, Y. α -Amidino Rhodium Carbenes: Key Intermediates for the Preparation of (E)-2-Aminomethylene-3-Oxoindoles and Pyranoidoles. *Org. Lett.* **2016**, *18*, 3682–3685.
- (80) Medeiros, M. R.; Schaus, S. E.; Porco, J. A. Jr. A Cycloisomerization/Friedel–Crafts Alkylation Strategy for the Synthesis of Pyrano[3,4-*b*]Indoles. *Org. Lett.* **2011**, *13*, 4012–4015.
- (81) Kuriyama, M.; Hamaguchi, N.; Yano, G.; Tsukuda, K.; Sato, K.; Onomura, O. Deuterodechlorination of Aryl/Heteroaryl Chlorides Catalyzed by a Palladium/Unsymmetrical NHC System. *J. Org. Chem.* **2016**, *81*, 8934–8946.
- (82) Fagan, P. J.; Ward, M. D.; Calabrese, J. C. Molecular Engineering of Solid-State Materials: Organometallic Building Blocks. *J. Am. Chem. Soc.* **1989**, *111*, 1698–1719.